Structures 78 (2025) 109344

Contents lists available at ScienceDirect

Structures

journal homepage: www.elsevier.com/locate/structures

Development of high-performance glulam beams of Pinus nigra with embedded CFRP for its application for a real case for structural rehabilitation

Carlos Cruz [a,*], Rafael Bravo [b], Francisco J. Rescalvo [b], Yaiza Fuentes-García [a], Francisco J. Lafuente-Bolívar [c], Antolino Gallego [a]

[a] Applied Physics Department, UIMA Laboratory, University of Granada, Campus de Fuentenueva s/n, Granada 18071, Spain
[b] Department of Structural Mechanics, UIMA Laboratory University of Granada, Campus de Fuentenueva s/n, Granada 18071, Spain
[c] Department of Architectural and Engineering Graphic Expression, UIMA Laboratory, University of Granada, Campus de Fuentenueva s/n, Granada 18071, Spain

ARTICLE INFO

Keywords:
Optimal design
Experimental tests
Analytical formulation longitudinal modulus
Shear modulus
Glulam beams
CFRP

ABSTRACT

This work presents the design, elaboration, analytical calculation and experimental results of laminated beams internally reinforced with pultruded carbon fiber (CFRP) of high mechanical performance. During the rehabilitation of the Chapel Courtyard of the Royal Hospital of the University of Granada (Head Office of the Rectorate), three sawn timber beams were found to be completely broken due to a high eccentric load. For this purpose, an exhaustive control was carried out to classify the lamellas that make up the laminated beams into three qualities according to their longitudinal modulus of elasticity measured by non-destructive tests. Once the beams were produced, elastic and non-destructive tests were carried out before and after embedding the reinforcement. Finally, one of the beams was subjected to a flexure to failure test as a control element, with the remaining beams being placed in the actual construction site. In addition, this work presents a novel method to calculate the static global modulus of elasticity with a formulation based on the strains recorded by strain gauges. In addition, an analytical formulation estimating the global shear modulus of the element is presented. The results show a considerable increase of the global modulus of elasticity due to the CFRP, improving the strength and ductility. Finally, the analytical results show a good correlation with the experimental results.

1. Introduction

The first signs of the use of wood in construction date back to the Mesolithic (12000–9000 BC), being reflected in the treatise "*de Arquitectura*" by Marco Vitruvio (25 BC), highlighting its beauty, strength, and usefulness as a building material and defining the qualities and uses of wood [1]. At the beginning of the 20th century, timber construction was based on round logs or sawn timber. This is why, structurally, the entire world heritage is made up of elements that include the natural imperfections of wood, such as knots and splits. When renovating a building (heritage or otherwise), a first response must be given whether the timber elements should be replaced or repaired [2]. In the case of the need for replacement, this becomes more complicated in the case of protected buildings, such as those included in the highest protection classification in Spain (BIC or *Bien de Interés Cultural*).

Today, structural engineered wood products (EWP) are widely used due to their excellent mechanical properties at a low weight [3]. The two most widespread products are glued laminated timber (GLT) and cross-laminated timber (CLT). These products allow the production of elements with greater structural uniformity, and therefore greater stiffness and strength [4]. The use of GLT for replacing sawn timber in historic buildings is a common practice [2]. However, in certain situations, due to the modifications that buildings undergo during their lifetime, structural elements can be subjected to high loads far beyond their original design [5]. This means that even the mere replacement by a conventional EWP such as GLT may not be sufficient due to the high mechanical performance required. In addition, the heritage protection limits the beam cross-section in base and height (the latter being the most critical as it cannot provide the beam with a higher inertia).

In this situation of high structural performance and section restriction of the slab element, new reinforcement solutions are emerging, such as the use of composite materials, see [6] for CFRP cords, or [7]and [8]

* Corresponding author.
E-mail address: carlos.cruz@ugr.es (C. Cruz).

https://doi.org/10.1016/j.istruc.2025.109344
Received 5 March 2025; Received in revised form 12 May 2025; Accepted 30 May 2025

for pultruded carbon fiber laminates or CFRP. The CFRP reinforcements have traditionally been mainly used in conventional reinforced concrete beams and slabs to strengthen and improve the flexural capacity. These include the use of discontinuous structural synthetic fibers (DSSF) [9,10], CFRP laminates with varying layer numbers [11] and transverse anchor strips [12], and CFRP cords [13], which offer improved compatibility and flexural performance. Furthermore, these reinforcement methods have shown enhanced load-bearing capacity under high-temperature conditions, where the mechanical properties of concrete tend to degrade [9,14]. Therefore, its application to timber is straightforward.

In timber the CFRP provides an optimum ratio between the lightness and high stiffness contribution, [15]. The introduction of these elements in the outer layers of the glued laminated beam [16] increases the compressive and tensile behaviour and the overall modulus of elasticity, as well as the ductility of the element [17] and [18]. However, visually, the fiber is exposed, which is a negative aesthetic aspect that is key and unfeasible for use in heritage buildings where the reinforced elements are exposed. For this reason, the solution of embedding the reinforcement in the production of the laminated beam arises, solving of this inconvenience and providing an effective reinforcement solution as shown by [19] and in the state of the art [20]. In recent years, the significant rise in structural loads and spans has led to an increase of the bonding length of CFRP, in some cases requiring the implementation of anchorage systems to secure the laminates. The studies conducted by [21] and [22] have experimentally and numerically confirmed the enhancement in load-bearing capacity provided by such anchorages. Furthermore, [23] have also demonstrated the structural improvement offered by the anchorage systems under dynamic impact loading conditions.

The main aim of this work is the structural rehabilitation of the historic Head Office of the University of Granada (Royal Hospital of Granada) through the use of glued laminated timber beams reinforced with carbon fiber-reinforced polymer (CFRP), employing local pine wood. Given the status of the building as a *Bien de Interés Cultural (BIC)*, which imposes the highest level of heritage protection in Spain, dimensional constraints were imposed. In response to these conditions, that is, i) high loads, ii) eccentric loading, and iii) strict cross-section limitations, the only viable solution that preserved the use of structural timber was the fabrication of high-performance glulam beams, internally reinforced with a CFRP plate and composed of high strength timber lamellas with optimally distributed along the cross section.

This paper presents the methodology and results of enhancing the mechanical performance of four custom-made CFRP-reinforced glulam beams, ad-hoc designed for the structural rehabilitation of a protected historical building. The reinforcement strategy presented in this work introduces two key innovations. First, the structural optimization of glulam beams is achieved through the strategic arrangement of lamellas based on non-destructive mechanical grading. This enables the placement of higher-stiffness lamellas in zones of maximum stress, enhancing the overall bending performance of the beam. Unlike previous approaches that rely on mixed-species configurations [24], 2022) or numerical metaheuristic optimization of lamella layout without experimental validation [25] the proposed method is experimentally verified to beams reinforced with carbon fiber-reinforced polymer (CFRP). The second innovation involves the development and experimental validation of two novel analytical models to estimate the global equivalent modulus of elasticity (MoE) and shear modulus (G) in glulam beams composed of lamellas with variable mechanical properties. The first model is based on the measurement of tension and compression strains, incorporating the different mechanical behavior of timber in tension and compression. The second model estimates the global shear modulus from the individual shear moduli of each lamella, obtained via non-destructive testing. Both models provide practical alternatives to conventional methods outlined in [26], such as the load-deflection approach or the torsion-based span methods.

Given the geometric limitations, the integration of an embedded CFRP laminate is essential to satisfy the bending requirements without increasing the cross-section of the beam. The process exposed in Section 3 involved: i) selection and grading of Pinus nigra boards from Andalusia via visual and non-destructive methods; ii) classification of lamellas into three stiffness grades and their optimized distribution in the cross-section; iii) fabrication of glulam beams with internal CFRP reinforcement; iv) full-scale flexural testing, including ultimate failure of one specimen and elastic testing of three beams installed on site; and v) final installation in the building. Alongside quality control through both destructive and non-destructive techniques, the proposed analytical models presented in Sections 3.6 and 3.7 provide practical tools for improving the accuracy of structural calculations that will help to discuss and interpret the results presented in Section 4.

2. General description of the historical building, the structural situation and pre-dimensioning

The Royal Hospital of Granada, founded in 1504, is currently the headquarters of the University of Granada. It is a building that is representative of a period of urban transformation from a Muslim city to a Christian city, within the context of the new state established by the Catholic Monarchs. From the 16th century onwards, the cross-shaped ground plan was introduced in Spain, and it was in the Granada hospital that the cross was completed for the first time with the four large courtyards [27].

It is a building with a Greek cross floor plan, inscribed in a square, which includes four courtyards in each of its corners, the courtyard of the Marbles, the courtyard of the Chapel (the site of the work), the courtyard of the Archive and the courtyard of the Innocents. In the upper porticoed gallery of this courtyard (east corner), with a clear Italian influence, is where the volume that is the subject of this work is located, which functionally arises as an access staircase to the outside of the roofs and dome of the building.

As shown in Fig. 1-a, this 7 t staircase is eccentric to the floor slab, causing a high bending moment and shear to the beams underneath it (Fig. 1-b). The three beams under the staircase collapsed, being the span between the supports equal to 3600 mm. As a BIC building (*Bien de Interés Cultural*, higher protection of the heritage in Spain), the beams could not increase in width (120 mm), and the maximum edge limit according to the intervention was 270 mm.

In order to establish the design of the glulam beams, predimensioning was carried out using the DLUBAL RFEM v5.30 program. The calculation showed that beams of strength class GL32c were not capable of meeting the required high mechanical performance, proving the need for the use of CFRP. In particular, the unreinforced beams resulted in a deflection and shear depletion ratio of 1.15 and 1.05 (1 being the maximum capacity limit). Based on previous work by our research group [18], the same calculation was performed for a CFRP-strengthened beam, resulting in values of 0.89 and 0.95, respectively.

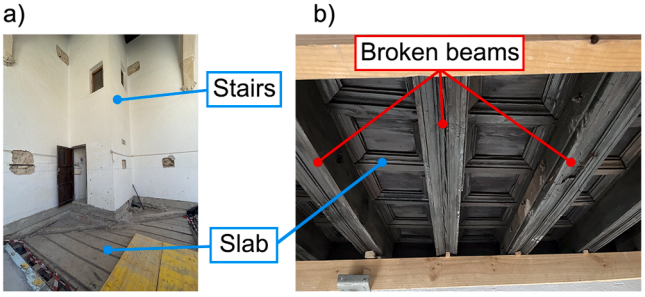

Fig. 1. a) Location of the staircase inside the wall b) Beams under the staircase totally fractured.

3. Materials and methods

3.1. Timber selection and characterisation

It was used wood from Laricio Pine or *Pinus nigra* of Andalusian origin (Monte de Navahondona-Parque Natural de Cazorla, Segura y las Villas), approximately 180 years old. Logs of 2500 mm in length were obtained, as shown in Fig. 2-a. The logs were transported to a local sawmill, where boards of dimensions 50 × 150 x 2500 mm were sawn. These boards were dried for 6 months under natural conditions, with adequate ventilation and protection from rain and direct sunlight. Once the moisture content (MC) was 11 ± 2 %, according to [28], 85 boards were visually selected that met the requirements of a visual class ME-1 according to the Spanish standard [29]. After visual selection, the wood was taken to our laboratory for mechanical characterisation using non-destructive methods. According to the method described in Section 3.4, longitudinal resonance acoustic tests were performed to obtain the dynamic modulus of elasticity or $MoE_{dyn,L}$ of all boards [30]. The values were corrected to 12 % MC according to the standard [28], obtaining the normal distribution curve shown in Fig. 2-b.

As can be seen, the $MoE_{dyn,L}$ values vary from 10500 to 18000 MPa, the mean value being 13869 MPa with a standard deviation of 1565 MPa. In terms of tensile strength class [31], variations were obtained from T13 to T30 (or higher), with more than 50 % of the boards above class T26. In order to verify this strength class, 20 tensile to failure tests were carried out on wood from the same batch, obtaining a failure strength of 53 MPa, equivalent to a T30 class.

3.2. FRP and epoxy adhesives

DRIZORO® COMPOSITE 1412 carbon fiber laminate (120 mm wide) was used as embedded reinforcement. This product is an epoxy matrix laminate obtained from a continuous and automated pultrusion process. Table 1 shows the main mechanical properties of the CFRP laminate.

MAXPRIMER-C primer was applied at 0.25 kg/m^2 to improve the wood-CFRP adhesion [32]. After drying the primer (24 h at 20° C and 50 % of relative humidity), the CFRP reinforcement was applied with MAXEPOX CS adhesive, applied at 0.6 kg/m^2.

3.3. Glulam beams: desing and manufacturing

According to the calculation, the base glulam (without CFRP) was required to be of class GL32c. Therefore, the T-class distribution defined [31] was employed. Specifically, the combination that differentiates between the outer, intermediate and inner laminate zones ([33]- Fig. 7) was applied, corresponding to the minimum classes T26, T18 and T11, respectively.

A total of 4 beams were produced, 3 to be tested in bending in the elastic range and placed on site and 1 to be tested to failure as a control.

Table 1
Mechanical characteristics of the CFRP Drizoro Composite.

Modulus of elasticity (GPa)	170
Thickness (mm)	1.4
Tensile strength (GPa)	2.60
Ultimate elongation (%)	1.60
Tensile strength for design (GPa)	1.32
Recommended elongation for design (%)	0.80

After cleaning the knots and defects, 36 lamellas with a cross-section of 40 × 140 and a length of 3600 mm were obtained using finger joints.

In order to optimise both the use of wood and the contribution of the reinforcement in terms of mechanical performance, two strategies were carried out: i) Design in glulam section by differentiating 3 strength grades, associated with the zones described by the [33]; ii) Place the CFRP reinforcement as close as possible to the face of maximum tensile efforts.

Regarding i), a cross-section design was established by differentiating 3 lamella qualities (Fig. 3-a) according to their $MoE_{dyn,L}$. These qualities are associated with the stress distribution, with the outer lamellas being the most stressed and therefore the ones with the highest modulus of elasticity or required quality (quality 1). A quality requirement of quality 2 was assigned to the immediately adjacent lamellas and, finally, quality 3 was assigned to the central lamellas. With the design and number of lamellae required by quality, non-destructive resonance tests were carried out to obtain their $MoE_{dyn,L}$, associating each lamella with a given quality (Fig. 3-b).

The modulus of elasticity ranges obtained were [11113–14674], [14729–16051] and [16163–18062] MPa for grades 3, 2, and 1, respectively. This translates into classes T14 to T26 for grade 3, classes T26 to T30 for grade 2, and class >T30 for grade 1. The 4 lamellas with the lowest elastic modulus were discarded, resulting in 32 final lamellas (8 per beam). The average value of the lamellae had a slight increase of 1.2 % (14050 MPa) compared to the values obtained in the sawn board.

As can be seen in Fig. 3-a, the lamella thickness on the maximum tensile face (L1) was set at 23 mm, compared to 32 mm for the other ones. This is due to strategy ii), allowing the reinforcement to provide the greatest possible mechanical improvement without compromising the integrity of the lamella itself. The final beam length was 3500 mm. In addition, the dynamic shear modulus of elasticity (G_{dyn}) of each lamella was measured by resonance testing, yielding a mean value of 935 MPa and a standard deviation of 192 MPa.

After grading and final machining of each lamella, the laminated beams were produced in two phases (Fig. 4). First, lamellas L2 to L8, with a final thickness of 32 mm, were glued and pressed (Phase 1- Fig. 4a). LOCTITE® HB S709 PURBOND polyurethane-based single-component adhesive was used for gluing. This adhesive was tested according to UNE-EN 15425 and classified as Type I for use in all service

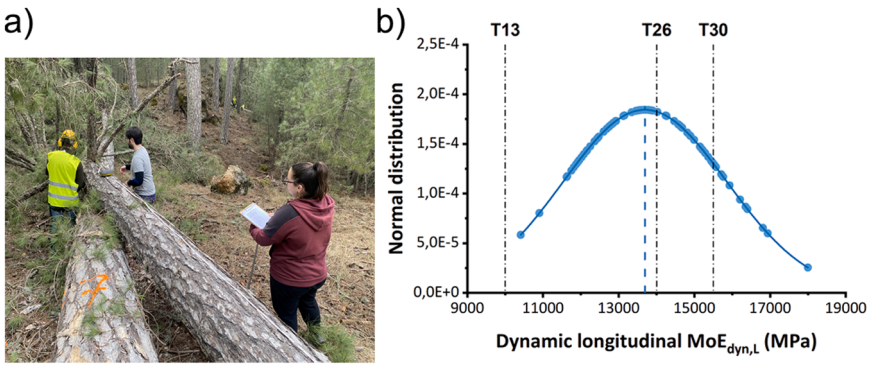

Fig. 2. a) Cutting of wood b) Normal distribution of the dynamic modulus of elasticity in sawn board. Discontinuous line: $MoE_{dyn,L}$ medium. Continuous line: T classes according to [31].

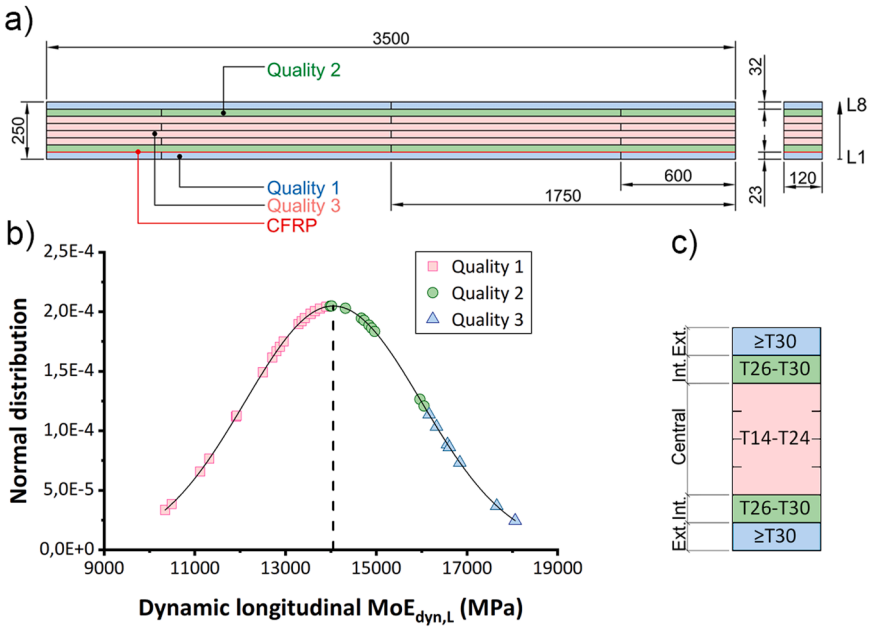

Fig. 3. a) Design of the laminated beam according to the lamella quality. b) Normal distribution of the dynamic modulus of elasticity for the lamellas. c) Association with each quality.

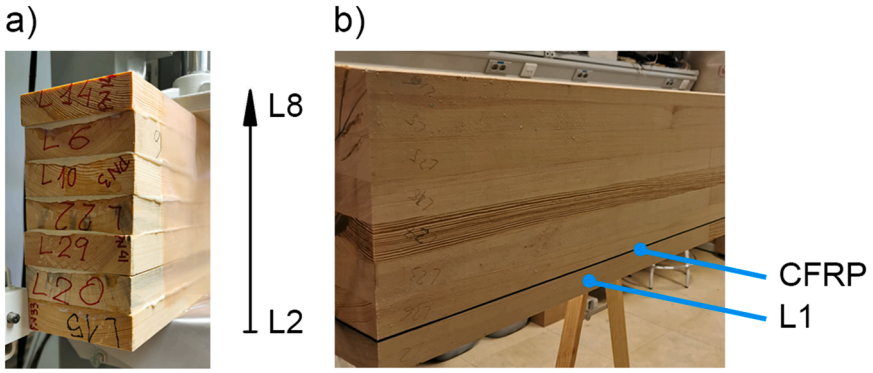

Fig. 4. Processing steps of the CFRP internally strengthened laricio pine beams. a) Phase 1. b) Phase 2.

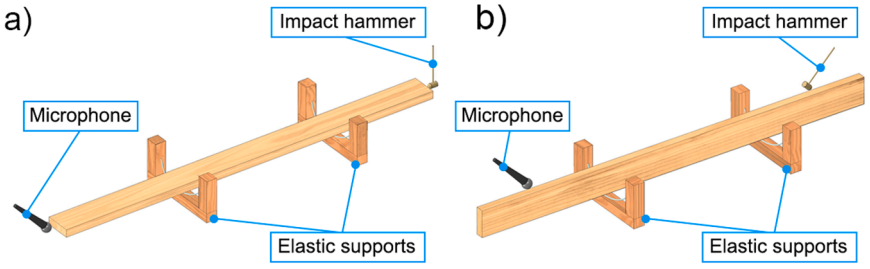

Fig. 5. Setup for the non-destructive resonance test (NDT). a) longitudinal test. b) transversal test.

classes. The adhesive has a viscosity of 24000 mPa-s (Brookifield 20 °C / 20 rpm, spindle 6), with resistance to weak alkalis, acids and solvents. The pressing was carried out in the STROMAB SL2 hydraulic press with a pressure of 1 N/mm^2. Finally, both the main body (L2 to L8) and the single lamella (L1) were subjected to 4-point bending tests in the elastic range (Section 3.5).

Phase 2 (Fig. 4.b): after curing of the adhesive, the CFRP plate and the wooden L1 lamella were bonded using MAXPRIMER - C primer on the contact faces, followed by MAXEPOX - CS epoxy resin.

Finally, a density of 541, 537, 562 and 545 kg/m3 was obtained for beams 1, 2, 3 and 4, respectively. In order to verify the quality of the bond between laminae, shear tests of glue line were carried out according to EN 14080- Annex D, obtaining a shear strength *fv* of 13.3 MPa with a wood failure greater than 98 %. This result comfortably meets the standard requirements (minimum shear strength of 6 MPa and minimum wood failure of 90 %).

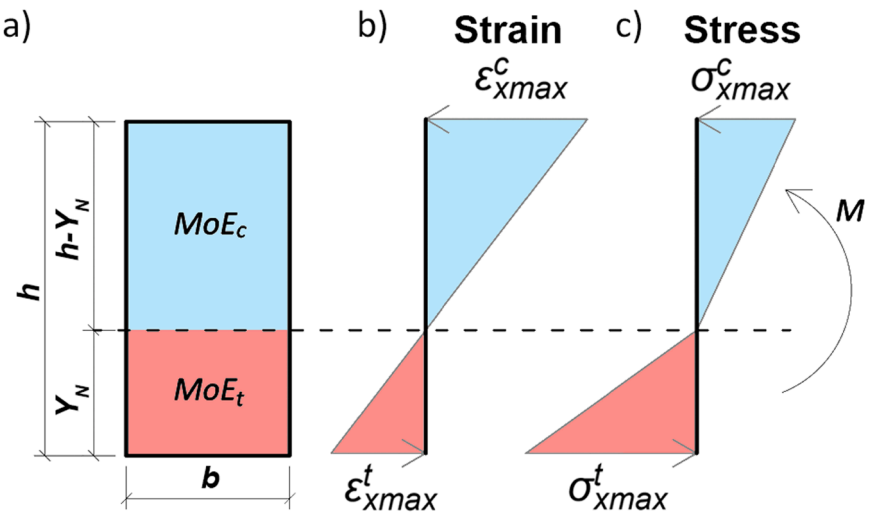

Fig. 6. Distributions of a section subjected to a bending moment M. a) rectangular timber cross-section with different moduli of elasticity in tension and compression. b) strain distribution. c) stress distribution.

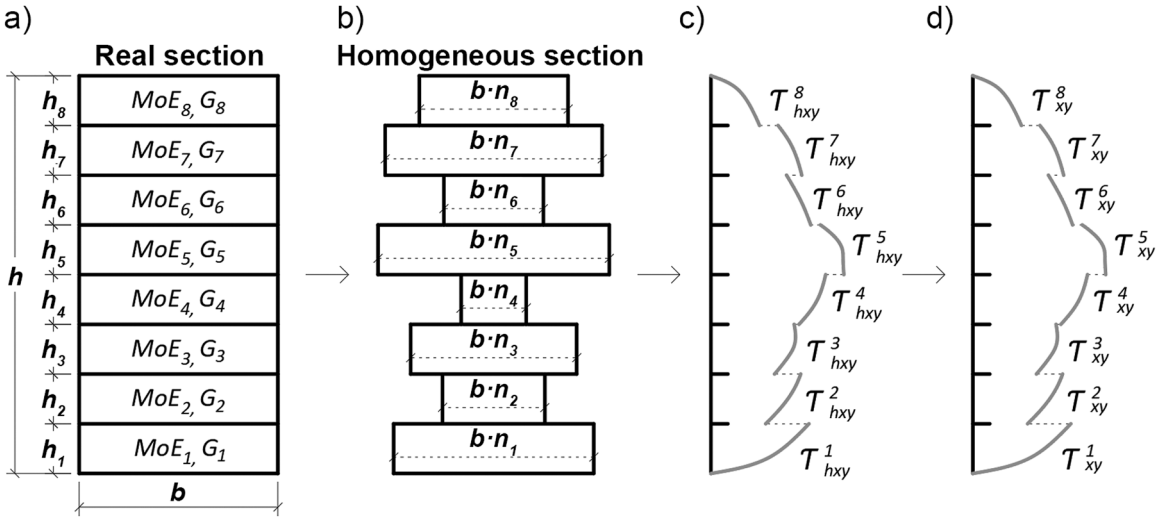

Fig. 7. a) Real section of study composed by 8 lamellas. b) homogenous section. c) shear stress distribution in the homogenous section. d) shear stress distribution in the real section.

3.4. Non-destructive testing (NDT). Estimation of the longitudinal and shear moduli of elasticity (MoE and G)

The non-destructive (NDT) acoustic resonance test was used to determine the longitudinal and shear moduli of elasticity. The hypothesis of the homogeneity of the geometrical and mechanical properties of the beam is considered, as well as the basic theorems of the longitudinal and transverse vibration dynamics. The tests were performed in longitudinal and transverse directions to the sawn timber boards and subsequently to the lamellas, and finally to the four manufactured beams. Fig. 5-a shows the setup for the longitudinal resonance test. Each sample (boards, lamellas, and beams) was placed on two elastic supports and subjected to free vibrations in the direction of the fibers (longitudinal test) or in the perpendicular direction (transversal test). The hit in both cases was applied with a timber hammer at one end and the microphone captured the elastic wave signal (T-bone MM-1 Thomann) at the other end. The signal was acquired by the oscilloscope (Picoscope® 4424 with 80 Ms/s maximum sampling frequency) from the microphone, and the data are analysed using the BING (Beam Identification by Non-Destructive Grading) software [30].

The $MoE_{dyn,L}$ is calculated using the Bernoulli model [11] according to the following Eqs. (1)-(2):

$$C_p = 2 \quad L_m \bullet f_1 \tag{1}$$

$$MoE_{dyn,l} = \rho_m \bullet C_p \tag{2}$$

where C_P is the propagation velocity of the stationary waves generated at the first frequency of resonance f_1, Lm is the length of the sample, and ρ_m is the density of the specimen. The moisture content was measured for each specimen, and then the $MoE_{dyn,L}$ was adjusted, using a relative moisture content of 12 % from [12] as the reference value.

For the transversal test, this software uses the theory proposed in [30], which is based on the bending resonance frequency and the Timoshenko bending theory to determine the transverse modulus of elasticity $MoE_{dyn,T}$ and the shear modulus G_{dyn} under free boundary conditions. To find G_{dyn}, the resonance motion of a beam as a first-order approximation is used in Eq. (3):

$$MoE_{dyn,T}/\rho_m = (MoE_{dyn,T}/KG_{dyn})X_n + Y_n \tag{3}$$

where, $MoE_{dyn,T}$ is the transverse dynamic modulus of elasticity in the

edgewise position, ρ_m is the density of the specimen, K is the shear factor with a value of $K = 5/6$ for a rectangular cross-section, and X_n and Y_n are parameters that depend on the mode of vibration.

To evaluate the real improvement of the CFRP in the glulam beam, NDT tests were carried out in the two phases of beam elaboration described in Fig. 4. and in reference [18]. From this, the modulus of elasticity and shear modulus of the main section (Phase 1, 7 lamellae) plus the L1 lamella were obtained. Applying the formulation from [34] based on the transformed section formulation and the Steiner theorem, the total $MoE_{dyn,L}$ of the beams without the CFRP reinforcement was estimated.

3.5. Static tests

All the beams were subjected to 4-point bending tests in the elastic range (Phases 1 and 2 of elaboration) according to [26], one of them being taken to rupture as a control element. The tests were carried out on a Microtest EM2/200 machine, which has an electric actuator with a maximum capacity of 200 kN. A displacement control speed of 12 mm/min was set. The distance between the supports and the distance between the load application points was established according to the standard [26]. The strains of the central section were measured using four HBM strain gauges, series K-CLY4–0100–1–120–3–005. Specifically, one was placed on the upper face (maximum compression), one on the lower face (maximum tension), and two lateral gauges on the L2 lamella. The latter allowed the position of the neutral fiber to be obtained. Of the four beams fabricated in accordance with the design conditions, the one with the lowest modulus of elasticity was selected and subjected to failure testing as the control specimen (beam 4). The remaining three beams were tested at 40 % of the maximum load reached by beam 4.

The static global modulus of elasticity MoE_{st} was calculated using the force-displacement relationship (F-w) between 10 % and 40 % of the maximum force, as prescribed by the standard [26](see Eq. 4). The maximum stress f_m was also calculated from the standard [26] (see Eq. 4). Where F is the maximum load of the only beam that could be tested to failure, *(a)* is the distance between the load cell and the nearest support, b is the width of the beam, and h is its depth.

$$MoE_{st} = \frac{3al^2 - 4a^3}{2bh^3\left(2\frac{w_2 - w_1}{F_1 - F_2} - \frac{6a}{5Gbh}\right)} \tag{4}$$

$$f_m = \frac{3Fa}{bh^2}; \sigma = \frac{F \cdot L}{b \cdot h^2}$$

3.6. Analytical approach for the computation of the equivalent longitudinal modulus elasticity of a timber section with different behaviour in tension and compression

The equivalent longitudinal modulus of elasticity MoE_{eq} of a timber section with different moduli of elasticity in tension MoE_t and compression MoE_c, (Fig. 6.a) can be computed through the strains measured in the tension ε^t_{xmax} (bottom) and compression ε^c_{xmax} (top) areas in the four point bending test (see Fig. 11.b). In an infinitesimal volume dV subjected to longitudinal stress σ_x, its strain energy dU is given by Eq. (5):

$$dU = 1/2\sigma_x\varepsilon_x dV = 1/2\sigma_x\varepsilon_x dx dA \tag{5}$$

The total energy per unit length in a cross-section of width b and height h subjected to a bending moment M that produces the stress-strain distributions depicted in Fig. 11. is Eq. (6):

$$\frac{dU}{dx} = 1/2\int_A \sigma_x\varepsilon_x dA = 1/2\int_{A^c} \sigma^c_x\varepsilon^c_x dA + 1/2\int_{A^t} \sigma^t_x\varepsilon^t_x dA \tag{6}$$

The maximum compression σ^c_{xmax} and tension σ^t_{xmax} stresses are computed according to [35] as function of M, MoE_t and MoE_c as Eq. (7):

$$\sigma^c_{xmax} = \frac{-3\left(1 + \sqrt{MoE_c/MoE_t}\right)}{bh^2}M, \text{and}\sigma^t_{xmax} = \frac{3\left(1 + \sqrt{MoE_t/MoE_c}\right)}{bh^2}M. \tag{7}$$

Taking into account that the position of the neutral axis Y_N can be defined according to [35] as a function of the moduli of elasticity in tension and compression as $Y_N = \frac{\sqrt{MoE_c}}{\sqrt{MoE_c}+\sqrt{MoE_t}}h$. Therefore, the maximum stresses can be expressed as Eq. (8):

$$\sigma^c_{xmax} = \frac{-3\left(1 + \frac{Y_N}{h-Y_N}\right)}{bh^2}M, \text{and}\sigma^t_{xmax} = \frac{3\left(1 + \frac{h-Y_N}{Y_N}\right)}{bh^2}M. \tag{8}$$

And their corresponding distributions are Eq. (9) ~ (10):

$$\sigma^c_x = \sigma^c_{xmax}\frac{y}{Y_N}, \quad \sigma^t_x = \sigma^t_{xmax}\frac{-y}{(h - Y_N)} \tag{9}$$

$$\varepsilon^c_x = \varepsilon^c_{xmax}\frac{y}{Y_N}, \varepsilon^t_x = \varepsilon^t_{xmax}\frac{-y}{(h - Y_N)}. \tag{10}$$

Additionally, Y_N can be computed with ε^c_{xmax} and ε^t_{xmax} as $Y_N = \frac{\varepsilon^t_{xmax}}{\varepsilon^t_{xmax} - \varepsilon^c_{xmax}}h$. Finally, the integrals in the compression and tension areas, and the total energy of the section are evaluated as Eqs. (11), (12)::

$$\int_{A^c} \sigma^c_x\varepsilon^c_x dA = \int_0^{h-Y_N} \frac{\sigma^c_{xmax}}{(h - Y_N)^2}\frac{\varepsilon^c_{xmax} b}{} y^2 dy = \frac{-\varepsilon^c_{xmax}}{h}M,$$

$$\int_{A^t} \sigma^t_x\varepsilon^t_x dA = \int_{-Y_N}^0 \frac{\sigma^t_{xmax}}{Y_N^2}\frac{\varepsilon^t_{xmax} b}{} y^2 dy = \frac{\varepsilon^t_{xmax}}{h}M. \tag{11}$$

$$\frac{dU}{dx} = \frac{1}{2}\int_{A^c} \sigma^c_x\varepsilon^c_x dA + \frac{1}{2}\int_{A^t} \sigma^t_x\varepsilon^t_x dA = \frac{\varepsilon^t_{xmax} - \varepsilon^c_{xmax}}{2h}M. \tag{12}$$

The energy of the same section with an equivalent material with equal moduli in tension and compression is given by Eq. (13):

$$\frac{dU}{dx} = \frac{1}{2}\int_A \sigma_x\varepsilon_x dA = \frac{bM^2}{2MoE_{eq}\ I^2}\int_A y^2 dA = \frac{3M^2}{MoE_{eq}\ bh^3} \tag{13}$$

Equating both energies, substituting the maximum moment of the four-point bending test M=Fa/2, the modulus of elasticity MoE_{eq} results as Eq. (14):

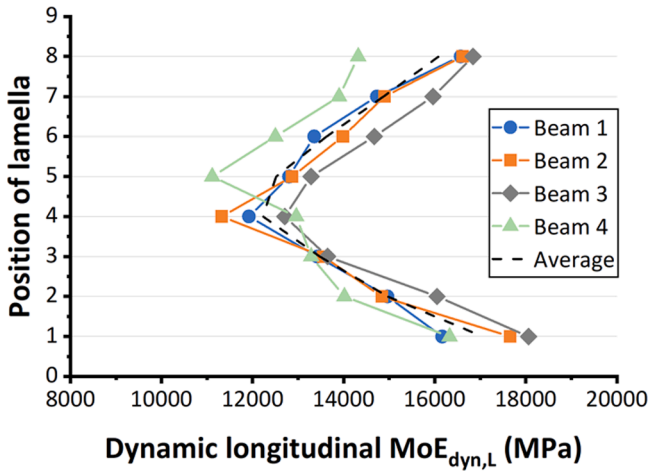

Fig. 8. Longitudinal dynamic modulus of elasticity of each beam according to the position of the lamella. Discontinuous black line: Mean value.

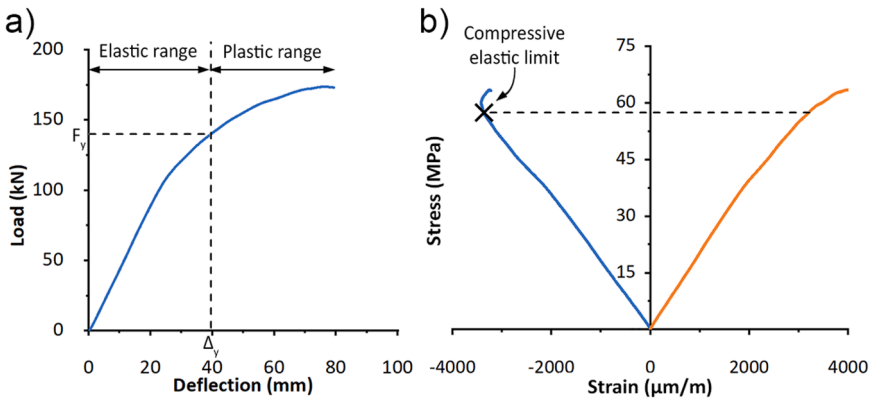

Fig. 9. 4-point bending test until failure of reinforced beam 4: a) Load-displacement diagram. b) Stress-strain diagram in tension (orange) and compression (blue).

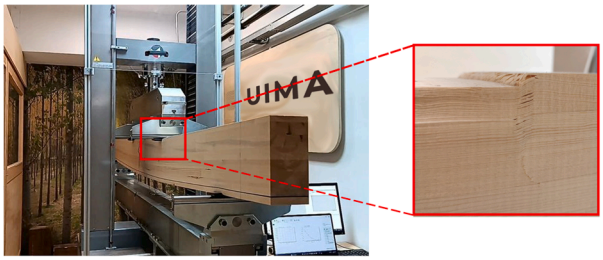

Fig. 10. Failure of the beam due to compression perpendicular to the grains.

$$MoE_{eq} = \frac{6M}{bh^2\left(\varepsilon^t_{xmax} - \varepsilon^c_{xmax}\right)} = \frac{3Fa}{bh^2\left(\varepsilon^t_{xmax} - \varepsilon^c_{xmax}\right)}. \quad (14)$$

Although the computation of this modulus comes from an analytical formulation, the authors called it as MoE_{eq} to denote that it is computed through the data (strains and moment) from four point bending static tests.

3.7. Analytical approach for the computation of the equivalent shear modulus G of a composite section

The equivalent shear modulus $G_{analytic}$ of a rectangular cross-section of width b and height h composed of N lamellas, each having a different thickness h_i, and shear modulus G_i, (Fig. 7.a), can be computed using the Transformed Section Method and the Parallel Axis Theorem, see [36]. Considering an infinitesimal volume dV subjected to shear stress τ_{xy}, then the strain energy dU can be calculated as Eq. (15):

$$dU = 1/2\tau_{xy}\gamma_{xy}dV = 1/2\tau_{xy}\gamma_{xy}dxdA \quad (15)$$

Where γ_{xy} is the shear strain. The total energy in a cross-section composed of N lamellas is Eq. (16):

$$\frac{dU}{dx} = 1/2\int_A \tau_{xy}\gamma_{xy}dA = 1/2\sum_{i=1}^{N}\int_{A_i}\tau^i_{xy}\gamma^i_{xy}dA_i. \quad (16)$$

The shear stress in a section composed of multiple materials is computed through the transformed section method converting the real section into a fictitious homogeneous section with modulus of elasticity MoE_h (Fig. 7.b). In the case of reinforced beams. the shear modulus of the CFRP laminate (out-of-plane) was obtained using the equations described in [37], taking into account a Poisson's ratio of 0.3 [37]. Applying the Collignon-Jourawski formulation [38] to the homogeneous section (Fig. 7.c), and transforming into the real ones, the shear stress τ^i_{xy} and shear strain γ^i_{xy} in a lamella i with modulus of elasticity MoE_i and shear modulus G_i are: $\tau^i_{xy} = n_i\frac{V_y S_{hi}}{b_{hi}I_{hi}}$ (Fig. 12.d), and $\gamma^i_{xy} = \frac{\tau^i_{xy}}{G_i}$. Where $n_i = MoE_i/MoE_h$ is the modular ratio, V_y is the shear force, $b_{hi} = n_i\ b_i$ is the width, S_{hi} is the static moment and I_{hi} is the moment of inertia, each of lamella i of the homogeneous section. Therefore, the energy can be written as Eq. (17):

$$\frac{dU}{dx} = \frac{1}{2}\sum_{i=1}^{N}\int_{A_i} n_i^2\frac{V_y^2 S_{hi}^2}{G_i b_{hi}^2 I_{hi}^2}dA_i = \frac{V_y^2}{2}\sum_{i=1}^{N}\frac{n_i^2}{G_i}\int_{A_i}\frac{S_{hi}^{z\,2}}{n_i b_{hi} I_{hi}^2}dy = \frac{V_y^2}{2}\sum_{i=1}^{N}\frac{n_i^2}{G_i A_{rhi}} \quad (17)$$

Where $\frac{1}{A_{rhi}} = \int_{A_i}\frac{S_{hi}^{z\,2}}{n_i b_{hi} I_{hi}^2}dy$ is the reduced area of lamella i in the homogeneous section. The energy of a section composed by an equivalent material Eq. (18):

$$dU/dx = \frac{V_y^2}{2G}\int_A \frac{S_z^2}{bI^2}dy = \frac{V_y^2}{2GA_r} \quad (18)$$

Equalling both energies, the following relation is obtained from Eq. (19):

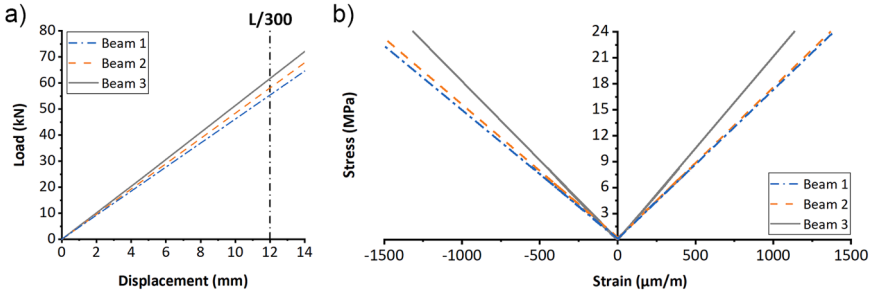

Fig. 11. Diagrams for 4-point bending tests in the elastic range of the reinforced beams 1, 2 and 3. a) Load -displacement curves. b) Stress-strain curves.

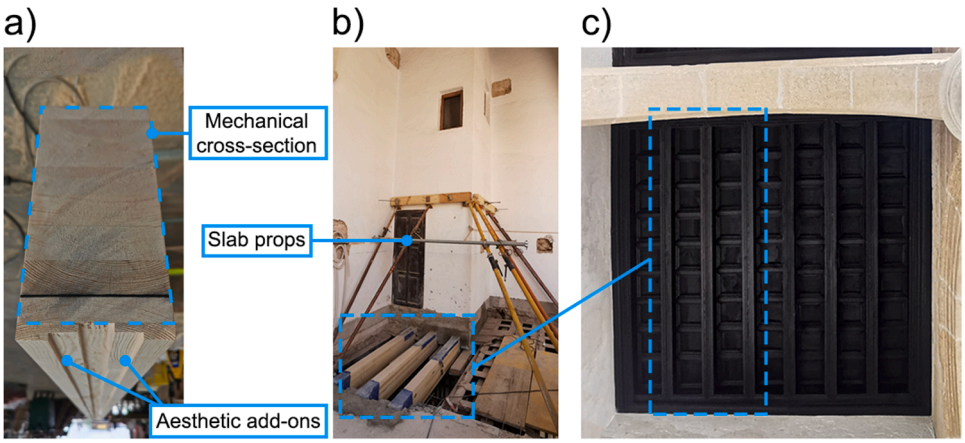

Fig. 12. Installation of the beams. a) Aesthetical stepped pieces. b) Placement of the beams on site and installation of the beams under the staircase. c) Bottom view of the floor slab after the final finishing of the beams.

$$\frac{V_y^2}{2}\sum_{i=1}^{N}\frac{n_i^2}{G_i A_{rhi}} = \frac{V_y^2}{2GA_r}, \tag{19}$$

and the shear modulus of the equivalent section is Eq. (20):

$$G_{analytic} = \frac{1}{A_r\sum_{i=1}^{N}\frac{n_i^2}{G_i A_{rhi}}}. \tag{20}$$

4. Results and discussion

Table 2 shows the final section distribution of the 8 lamellas that make up each beam, identifying their position of the lamella (PL) and assigned quality (Q), dynamic shear modulus G_{dyn}, dynamic longitudinal modulus of elasticity and the corresponding T class (TC) according to [33].

The dynamic modulus of elasticity (MoE_{dyn}) of each lamina comprising the cross-section of each beam is presented in Fig. 8. and Table 2, all beams met the minimum requirements of the combined glulam standard to achieve a GL32c strength class. The 4 beams follow a similar trend in their $MoE_{dyn,L}$ distribution according to the position of the lamella, corroborating the correct design of the beams and the quality association. The central lamellas (L4 and L5) have the lowest modulus, making them coincide by design with the position of the neutral fiber.

For qualities 1 and 2, an average $MoE_{dyn,L}$ of 16569 and 14920 MPa was obtained, respectively, which represents an increase of 28 % and 15 % with respect to the average value of quality 3, respectively. As for the dynamic shear modulus, as expected, no differences were observed between the qualities, with average values of 952, 949 and 941 MPa for qualites 1, 2 and 3, respectively.

Table 3 shows the obtained static (MoE_{st}), resonance (MoE_{dyn}), and analytical (MoE_{eq}) moduli of elasticity for the unreinforced and reinforced beams. In addition, the dynamic and analytical shear modulus (G_{dyn} and $G_{analytic}$, respectively) are included. The properties of the beams before strengthening were obtained according to the methodology described in Sections 3.4, 3.5, 3.6 and 3.7.

These results are in agreement with the design phase presented previously (Table 2), with beam 3 being the only one with a T30 grading for its L1, L2, L7 and L8 laminae. These laminae represent 48 % of the cross-section, with laminae L1 and L2 being in the bottom 22 % (maximum tensile) and laminae L7 and L8 in the top 26 % (maximum compressive). For the remaining beams, L2 and L7 laminae are graded T26/T24 according to design. This shows that a proper pre-section design phase with a classification of the laminae allows optimisation of the overall mechanical properties of a laminated beam. Looking at the average modulus of elasticity values, the three moduli obtained are similar, with the equivalent modulus (MoE_{eq}) being slightly higher (1.9 % with respect to MoE_{st}). All the beams exceeded the minimum value of 13500 MPa established by the standard for a GL32c beam.

In terms of the shear modulus, Table 3 shows that G_{dyn} is similar between the beams, with an average value of 1014 MPa. Here again, this

Table 2
Position and quality (POS/Q), dynamic shear modulus G_{dyn}, dynamic longitudinal modulus of elasticity $MoE_{dyn,L}$, and strength T class (TC) of each lamella.

	Beam 1			Beam 2			Beam 3			Beam 4		
POS/Q	G_{dyn} (MPa)	$MoE_{dyn,L}$ (MPa)	TC	G_{dyn} (MPa)	$MoE_{dyn,L}$ (MPa)	TC	G_{dyn} (MPa)	$MoE_{dyn,L}$ (MPa)	TC	G_{dyn} (MPa)	$MoE_{dyn,L}$ (MPa)	TC
PL8/Q1	728	16570	T30	855	16612	T30	820	16842	T30	1356	14319	T26
PL7/Q2	847	14729	T26	1054	14898	T26	1030	15962	T30	864	13900	T24
PL6/Q3	1236	13354	T21	874	13983	T24	828	14674	T26	1125	12499	T18
PL5/Q3	993	12801	T18	522	12871	T18	724	13284	T21	774	11113	T14
PL4/Q3	999	11921	T16	1110	11319	T14	1098	12706	T18	950	12959	T18
PL3/Q3	841	13424	T21	1026	13551	T24	1167	13646	T24	796	13285	T21
PL2/Q2	1224	14964	T26	943	14838	T26	775	16051	T30	855	14015	T26
PL1/Q1	1088	16163	T30	907	17657	T30	1214	18062	T30	646	16326	T30

Table 3
Non-reinforced and reinforced beams. Moduli of elasticity by the four-point bending test MoE_{st}, dynamic longitudinal modulus of elasticity $MoE_{dyn,L}$, MoE_{eq} with formulation from Section 3.6, dynamic shear modulus G_{dyn} and shear modulus by the analytical formulation from Section 3.7 $G_{analytic}$ for the four beams.

	Non-reinforced					Reinforced (variation respect to NR in %)				
Beam	MoE_{st} (MPa)	MoE_{dyn} (MPa)	MoE_{eq} (MPa)	G_{dyn} (MPa)	$G_{analytic}$ (MPa)	MoE_{st} (MPa)	MoE_{dyn} (MPa)	MoE_{eq} (MPa)	G_{dyn} (MPa)	$G_{analytic}$ (MPa)
1	14367	14530	14721	1012	1010	17424 (21 %)	14854 (2 %)	17055 (16 %)	1056 (4 %)	1017 (0,6 %)
2	14626	14642	14983	957	833	17498 (20 %)	15488 (6 %)	17414 (16 %)	1017 (6 %)	843 (1,2 %)
3	14996	15325	15606	1043	921	17421 (16 %)	16066 (5 %)	18075 (16 %)	968 (−7 %)	924 (0,4 %)
4	14068	13668	13897	1044	892	15501 (10 %)	14651 (7 %)	15782 (14 %)	1132 (8 %)	893 (0,1 %)
Mean	14514	14541	14802	1014	914	16961 (17 %)	14854 (5 %)	17082 (15 %)	1043 (4 %)	919 (0,6 %)
Error Std	394	680	708	41	74	974	642	964	69	73

is consistent with the design phase (Table 2), as the laminae were randomly positioned for this mechanical property. For the analytical shear modulus, a difference of up to 17 % (beam 4) is obtained with respect to the dynamic measurement. According to the Collignon-Jarowski formulation [36], the internal lamellas have a large influence on the shear modulus of the beam. Note that the individual moduli of these lamellas (L3 to L6) in each beam are very similar to the overall analytical value obtained. This is clearly marked in beam 2, with a difference in $G_{analytic}$ of 21 % compared to beam 1 due to the 522 MPa of the L5 lamella. For all beams, the G value obtained is higher than the 650 MPa required at [33]for a GL32c beam.

Table 3 also shows the elastic properties obtained after reinforcement and their respective percentage changes compared to the unreinforced beams. In general, all the moduli of elasticity improve when the beams are strengthened. In particular, the static modulus increased by up to 21 % (beam 1), with an average value of MoE_{st} for the 4 beams of 16961 MPa. This value is 26 % higher than the value required by the standard [33] for a GL32c beam. Looking at the $MoE_{dyn,L}$, there is hardly any improvement compared to the strengthened beams, with an average variation of 5 %. This effect has been previously verified [30], due to the fact that the CFRP plate has a small cross-section, making it impossible for non-destructive techniques to evaluate the improvement in stiffness that it brings to the overall beam. Applying the formulation developed in Section 3.6, values very similar to MoE_{st} are obtained, with an average variation of only 0.7 %.

Table 4 shows the equivalent modulus of elasticity values given in Table 3, the relative position of the neutral fiber with respect to the bottom face (Y_N/h) in %, as well as the respective tensile and compressive elastic moduli and their respective variations with respect to the overall equivalent modulus for the beams before and after reinforcement. Compared to the unreinforced beams, in all cases the neutral fiber is slightly below the centre of the cross-section (50 %). This is due to the symmetry by design carried out in the production of the glulam beams (Table 2). In the design phase, Fig. 8 shows that due to the symmetry in the quality distribution, the neutral fiber should be around 50 % of the cross-section, a fact that is corroborated by the results in Table 4. In particular, the neutral fiber obtained from the strain gauges only shifts downwards by 1.3 % in the unreinforced beams. This symmetry is observed in the tensile and compressive moduli of elasticity obtained using the strain gauges, with a variation between them of 11 %. Similarly, the variation of the tensile and compressive moduli of elasticity with respect to the MoE_{eq} obtained maintains the aforementioned symmetry, with a slight overall difference of less than 6 %.

After applying the reinforcement to the beams, the neutral fiber decreases to 44 % of the total cross-section. This effect is logical due to the presence of the reinforcement on the tension face. This translates into an improvement in the average tensile modulus of elasticity of 14.5 % compared to the beams before reinforcement. Although lower, the compressive modulus of elasticity is improved by an average value of 5.4 %. The greatest improvement after the application of the compression stiffening occurs in beam 4, with an increase of 15 %. Looking at Table 2 (beam design), beams 1–3 have an average $MoE_{dyn,L}$ in the compression block (L5 to L8) of 14364, 14591 and 15191 MPa, respectively, while for beam 4 this block has an average value of 12958 MPa, 12 % lower. Therefore, even in compression, carbon fiber provides a greater improvement in the case of elements with a lower

Table 4
Non-reinforced and reinforced beams. Modulus of elasticity by the formulation of Section 3.6 MoE_{eq}, the relative position of the neutral axis to the total height Y_n /h, tensile and compressive moduli of elasticity MoE_{ten} and MoE_{comp}, and variation with respect to MoE_{eq}. All these values were computed from the formulation presented in [35]and [34]. Mean values and standard deviation.

	Non-reinforced						Reinforced (variation respect to NR in %)					
Beam	MoE_{eq} (MPa)	Y_n/h (%)	MoE_{ten} (MPa)	Moe_{comp} (MPa)	$\Delta MoE_{ten\text{-}eq}$ (%)	$\Delta Moe_{comp\text{-}eq}$ (%)	MoE_{eq} (MPa)	Y_n/h (%)	MoE_{ten} (MPa)*	Moe_{comp} (MPa)*	$\Delta MoE_{ten\text{-}eq}$ (%)	$\Delta Moe_{comp\text{-}eq}$ (%)
1	14721	49.1	15260	14210	3.7	−3.5	17055	44.9	17876 (17.1 %)	15403 (8.4 %)	4.8	−9.7
2	14983	48.4	16015	14048	6.9	−6.2	17414	44.8	18779 (17.2 %)	13745 (−2.1 %)	7.8	−21.1
3	15606	48.6	16510	14774	5.8	−5.3	18075	44.9	19130 (15.8 %)	14953 (1.2 %)	5.8	−17.3
4	13897	48.6	14718	13143	5.9	−5.4	15782	43.9	15779 (7.2 %)	15112 (14.9 %)	0	−4.2
Mean	14802	48.7	15626	14044	5.6	−5.1	17082	44.6	17891 (14.5 %)	14803 (5.4 %)	4.6	−10.9
Error Std	708	0.3	794	676	1.4	1.2	964	0.5	1504	730	2.9	6.6

* Variation with respect to the non-reinforced beams

modulus of elasticity [32]. The asymmetry of the reinforcement is highlighted in the variation of the modulus of elasticity in tension and compression with respect to the overall modulus obtained, being 4.6 % and 10.9 %, respectively.

Beam 4 was designed to be tested to failure as a control element, serving as a verification for the rest of the mechanical properties. Fig. 9-a shows the load-displacement relationship, showing a clear ductile behaviour. On the other hand, Fig. 9-b shows the stress-strain relationship recorded by the gauges placed at the maximum tension and compression. As expected, the observed ductility is because the carbon fiber allows the timber to reach its elastoplastic range in compression, as demonstrated in previous works [18,39,40]. Following the [41] standard, the design ductility was calculated and the yield strength was set at a load *Fy* of 140 kN and a displacement *Δy* of 39.76 mm as seen Fig. 9-a. This load translates into a bending strength of 51 MPa, which is 59 % higher than the GL32c strength class. After this limit, the beam in the elastoplastic range reached a maximum load of 170 kN (62 MPa) as observed in Fig. 9-b. The obtained ductility (structural safety) was 2.53, obtaining values similar to those of previous works [18]. Finally, the beam failed in compression perpendicular to the fiber (Fig. 10) at the load application points, even with the use of stress distribution lamellas. This is due to the CFRP plate, which allowed the full elastoplastic capacity of the timber to be mobilised in compression.

After the failure test, an elastic range test was carried out on the 3 beams to be placed on site. Fig. 11-a shows the load-displacement measured with LVL at the middle section of the reinforced beams, and Fig. 11-b shows the stress-strain relationships of the strain gauges placed in the tension and compression sides. Table 5 includes non-reinforced and reinforced loads for 12 mm (limit service state according to [42]) deflection and initial stiffness for beams 1–4, post-cracking stiffness, energy absorption pre-cracking and post-cracking of beam 4. In all cases, an expected linear behaviour is observed. The reinforcement increases the load capacity in average 23 %, similar increase is obtained for the initial stiffness. For the stress-strain slope of the tensile strain gauge is slightly higher than its compressive counterpart, thanks to the contribution of the CFRP. The beam 4 has energy absorption pre-cracking of 3198 J and a post-cracking of 148 J, while stiffness is reduced up to 51 %

5. Installation of the reinforced glulam beams

Subsequent to the mechanical testing in Section 4, two 15 mm aesthetical stepped pieces were added to beams 1, 2 and 3 (Fig. 12-a) on bottom face. Due to the high heritage protection of the building, the bottom face of the beams had to have a similar (but not identical) appearance to the existing beams. After this, the loads from the staircase were transferred to the perimeter walls by means of slab props (Fig. 12-b). Subsequently, the existing broken beams were then removed and the wall joints were thoroughly cleaned. After that, the heads of the beams were covered with a Divoroll® waterproofing laminae, covering 400 mm inwards from the head of the beam (according to the technical data sheet). Fig. 12-c shows an image of the bottom of the slab after its final painting in accordance with the rest of the slabs and beams.

6. Conclusions

In this work, it has been successfully demonstrated that it is possible to meet highly demanding structural requirements through two main strategies: 1) optimisation of the quality of wood in the cross section, and 2) use of carbon fiber embedded in tension. Both technological strategies have made it possible to respond to a complex situation in the refurbishment of the courtyard of the Royal Hospital, headquarters of the Rectorate of the University of Granada, which is key to the proper conservation of the architectural heritage, as well as to the valorisation of the local timber resource. These strategies enabled the development of high-performance beams from Andalusian Pinus nigra, capable of meeting strict structural and heritage constraints through enhanced flexural stiffness and ductility. Internally reinforced laminated beams of Andalusian pine have been developed with a high global elastic modulus, improving their tensile behaviour, as well as preventing brittle failure thanks to the elastoplastic mobilization of the laminated beam block subjected to compression. This solution is particularly relevant in historic buildings where dimensional limitations prevent conventional reinforcement strategies. Moreover, the use of CFRP reinforcement in timber takes advantage of the well-established and long-standing experience of fiber-based or CFRP reinforcement in concrete structures, which has been extensively studied under a wide range of conditions.

Non-destructive testing has proven to be an ideal technique to establish a demanding design in a glulam section. The design with three clearly differentiated qualities has allowed optimizing the resource and achieving a basic glulam beam that complies with the GL32c strength class standard. This design has been corroborated with experimental tests and analytical formulations, the latter providing an excellent correlation with the experimental section. Moreover, the strong agreement between experimental data and the novel analytical models proposed confirms their reliability for practical application in structural timber engineering. An experimental methodology was carried out using non-destructive techniques and 4-point testing in the elastic range that allowed the evaluation of the improvement introduced by the application of CFRP in the same beam before and after being reinforced, providing results with greater reliability. The use of CFRP between L1 and L2 (glue line at maximum tension) improved the maximum load on average a 23 %, the flexural behaviour between 10 % and 21 %. In addition, the ductility of the laminated beam was increased to a value of about 47 %, similar to previous research [39], with respect to the brittle behaviour experienced by an unreinforced laminated beam. These values highlight the effectiveness of embedded CFRP in achieving not only stiffness enhancement but also increased structural safety through greater energy absorption.

Table 5
Non-reinforced and reinforced loads for 12 mm deflection and initial stiffness for beams 1–4. Post-cracking stiffness, energy absorption pre-cracking and post-cracking of beam 4.

Loading conditions (kN) for a 12 mm deflection (L/300 – [42])			Maximum load conditions			
Beam	**Non-reinforced**	**Reinforced**	**Initial Stiffness (kN·mm)**	**Post-cracking Stiffness (kN·mm)**	**Energy Absorption Pre-cracking (J)**	**Energy Absorption Post-cracking (J)**
1	46	55 (21 %)	4,6	–	–	–
2	47	58 (24 %)	5,2	–	–	–
3	48	62 (29 %)	4,8	–	–	–
4	45	52 (17 %)	4,5	2,2 (−51 %)	3198	148
Mean	**46**	**57 (23 %)**	**4,8**	–	–	–
Std. Dev.	**1**	**4**	**0,3**	–	–	–

Both the application and the proposed solution have been widely disseminated within the sector (architects, engineers, builders). In particular, a great deal of interest has been shown in order to be able to carry out calculations of wood-CFRP products in a manageable way. The observed interest emphasizes the practical need for simplified and accurate design tools for CFRP-reinforced timber elements. Therefore, this research will be extended by the development of a software using artificial intelligence (AI) in order to make the calculation of these elements feasible, to optimise all resources and to adapt to the structural complexities of this type of projects. This future development aims to support decision-making in real projects with high structural and cultural demands, enabling the broader implementation of optimized timber-CFRP solutions.

Funding

This work was supported by the SMARTTIMBER project "Productos estructurales inteligentes de madera multiespecie para construcción industrializada baja en carbono", PID2020.114386RB.I00; the LIGHT-TIMBER project "Cajones estructurales de madera técnica aligerada para una construcción de baja huella ecológica", TED2021–130039B-I00; and the GLUCAR project "Pine-poplar-carbon fibre mixed glulam beams of high performance with laminated optimized by using artificial inteligent", PID2023–148379OA-I00.

CRediT authorship contribution statement

Cruz Rodriguez Carlos: Writing – original draft, Formal analysis, Data curation. **Antolino Gallego:** Writing – review & editing, Project administration, Funding acquisition. **Rafael Bravo:** Writing – review & editing, Supervision, Formal analysis. **Francisco J. Rescalvo:** Supervision, Methodology, Investigation, Conceptualization. **Yaiza Fuentes-García:** Writing – original draft, Formal analysis, Data curation. **Francisco J. Lafuente-Bolívar:** Supervision, Investigation, Conceptualization.

Declaration of Competing Interest

The authors declare that they have no known competing financial interests or personal relationships that could have appeared to influence the work reported in this paper.

Acknowledgements

Acknowledgement is due to Drizoro for the supply of reinforcement and "Vicerectorado de Patrimonio" of University of Granada.

References

[1] M.Vitrubio Polión, Delfín. Rodríguez Ruiz, J.L.Oliver Domingo, Los diez libros de arquitectura, 1a. ed. en Alianza Forma, 5a. reimp, Alianza, Madrid, 2006.
[2] Franke S, Franke B, Harte AM. Failure modes and reinforcement techniques for timber beams – State of the art. Constr Build Mater 2015;97:2–13. https://doi.org/10.1016/j.conbuildmat.2015.06.021.
[3] Wood Handbook, Wood as an Engineering Material, Centennial Edition, Madison, Wisconsin, 2010.
[4] Wang Q, Wang Z, Feng X, Zhao Y, Li Z. Mechanical properties and probabilistic models of wood and engineered wood products: a review of green construction materials. Case Stud Constr Mater 2024;21:e03796. https://doi.org/10.1016/j.cscm.2024.e03796.
[5] Biscaia HC, Chastre C, Cruz D, Franco N. Flexural strengthening of old timber floors with laminated carbon fiber–reinforced polymers. J Compos Constr 2017;21:04016073. https://doi.org/10.1061/(ASCE)CC.1943-5614.0000731.
[6] Fossetti M, Minafò G, Papia M. Flexural behaviour of glulam timber beams reinforced with FRP cords. Constr Build Mater 2015;95:54–64. https://doi.org/10.1016/j.conbuildmat.2015.07.116.
[7] De La Rosa García P, Escamilla AC, Nieves González García M. Bending reinforcement of timber beams with composite carbon fiber and basalt fiber materials. Compos Part B: Eng 2013;55:528–36. https://doi.org/10.1016/j.compositesb.2013.07.016.
[8] Nadir Y, Nagarajan P, Ameen M, Arif M M. Flexural stiffness and strength enhancement of horizontally glued laminated wood beams with GFRP and CFRP composite sheets. Constr Build Mater 2016;112:547–55. https://doi.org/10.1016/j.conbuildmat.2016.02.133.
[9] Al-Rousan RZ. Influence of polypropylene fibers on the flexural behavior of reinforced concrete slabs with different opening shapes and sizes. Struct Concr 2017;18:986–99. https://doi.org/10.1002/suco.201600222.
[10] Al-Rousan RZ. Influence of macro synthetic fibers on the flexural behavior of reinforced concrete slabs with opening. Civ Eng J 2022;8:2001–21. https://doi.org/10.28991/CEJ-2022-08-09-016.
[11] Al-Rousan RZ. Effect of CFRP schemes on the flexural behavior of RC beams modeled by using a nonlinear finite-element analysis. Mech Compos Mater 2015;51:437–46. https://doi.org/10.1007/s11029-015-9515-6.
[12] Alhassan M, Al-Rousan R, Ababneh A. Anchoring of the main CFRP sheets with transverse CFRP strips for optimum upgrade of RC beams: parametric experimental study. Constr Build Mater 2021;293:123525. https://doi.org/10.1016/j.conbuildmat.2021.123525.
[13] Al-Rousan RZ. Influence of opening sizes on the flexural behavior of heat-damaged reinforced concrete slabs strengthened with CFRP ropes. Case Stud Constr Mater 2022;17:e01464. https://doi.org/10.1016/j.cscm.2022.e01464.
[14] Al-Rousan RZ. Anchored CFRP ropes for flexural capacity recovering of thermally damaged RC one-way slabs. Alex Eng J 2023;76:757–74. https://doi.org/10.1016/j.aej.2023.06.086.
[15] Rescalvo FJ, Suarez E, Abarkane C, Cruz-Valdivieso A, Gallego A. Experimental validation of a CFRP laminated/fabric hybrid layout for retrofitting and repairing timber beams. Mech Adv Mater Struct 2019;26:1902–9. https://doi.org/10.1080/15376494.2018.1455940.
[16] Glišović I, Stevanović B, Todorović M, Stevanović T. Glulam beams externally reinforced with CFRP plates. Wood Res 2016;61.
[17] He M, Wang Y, Li Z, Zhou L, Tong Y, Sun X. An experimental and analytical study on the bending performance of CFRP-reinforced glulam beams. Front Mater 2022;8:802249. https://doi.org/10.3389/fmats.2021.802249.
[18] Rescalvo FJ, Timbolmas C, Bravo R, Valverde-Palacios I, Gallego A. Improving ductility and bending features of poplar glued laminated beams by means of embedded carbon material. Constr Build Mater 2021;304:124469. https://doi.org/10.1016/j.conbuildmat.2021.124469.
[19] Donadon BF, Mascia NT, Vilela R, Trautwein LM. Experimental investigation of glued-laminated timber beams with Vectran-FRP reinforcement. Eng Struct 2020;202:109818. https://doi.org/10.1016/j.engstruct.2019.109818.
[20] Al-Mashgari H, Liu X, Ngyuen T, Ngo T. Performance, methodology and opportunities in FRP strengthening techniques for timber structures: a state-of-the-art review. J Build Eng 2024;98:111073. https://doi.org/10.1016/j.jobe.2024.111073.
[21] Karagoz ileyen ÜK, Ghoroubi R, Mercimek Ö, Anil Ö, Abdullah T, Tugrul ER. Effect of anchorage number and CFRP str. Adv Struct Eng 2021;24. https://doi.org/10.1177/1369433220988622.
[22] İşleyen ÜK, Ghoroubi R, Mercimek Ö, Anil Ö, Erdem RT. Behavior of glulam timber beam strengthened with carbon fiber reinforced polymer strip for flexural loading. J Reinf Plast Compos 2021;40:665–85. https://doi.org/10.1177/0731684421997924.
[23] İşleyen ÜK, Ghoroubi R, Mercimek Ö, Anil Ö, Erdem RT. Investigation of impact behavior of glulam beam strengthened with CFRP. Structures 2023;51:196–214. https://doi.org/10.1016/j.istruc.2023.03.038.
[24] Danzer M, Dietsch P, Winter S. Effect of shrinkage on cracking and structural behaviour of reinforced glulam members. Constr Build Mater 2022;327:125977. https://doi.org/10.1016/j.conbuildmat.2021.125977.
[25] Pech S, Kandler G, Lukacevic M, Füssl J. Metamodel assisted optimization of glued laminated timber beams by using metaheuristic algorithms. Eng Appl Artif Intell 2019;79:129–41. https://doi.org/10.1016/j.engappai.2018.12.010.
[26] UNE 408–2011+A1_Estructuras de madera. Madera aserrada y madera laminadad encolada para uso estructural, (n.d.).
[27] Lubelza CFélez. El Hospital Real. Granada: Editorial Universidad de Granada; 2014.
[28] UNE-EN 384_2016+A1_Madera Estructural_Determinanción de densidad, propiedades mecánicas, (n.d.).
[29] UNE_56544–2022_Clasificación visual de la madera aserrada para uso estructural_Madera de coníferas, (n.d.).
[30] Brancheriau L, Bailleres H. Natural vibration analysis of clear wooden beams: a theoretical review. Wood Sci Technol 2002;36:347–65. https://doi.org/10.1007/s00226-002-0143-7.
[31] UNE 338_2016_Madera Estructural_Clases resistentes, (n.d.).
[32] Rescalvo FJ, Aguilar-Aguilera A, Suarez E, Valverde-Palacios I, Gallego A. Acoustic emission during wood-CFRP adhesion tests. Int J Adhes Adhes 2018;87:79–90. https://doi.org/10.1016/j.ijadhadh.2018.09.007.
[33] UNE-EN 14080_Estructuras de madera_Madera laminada encolada y madera maciza encolada, (n.d.).
[34] Timbolmas C, Bravo R, Rescalvo FJ, Portela M. Transformed-section method applied to multispecies glulam timber beams subjected to pure bending. Mech Adv Mater Struct 2022;29:6814–23. https://doi.org/10.1080/15376494.2021.1985665.
[35] Timbolmas C, Bravo R, Rescalvo FJ, Gallego A. Development of an analytical model to predict the bending behavior of composite glulam beams in tension and compression. J Build Eng 2022;45:103471. https://doi.org/10.1016/j.jobe.2021.103471.
[36] S. Timoshenko, Strength of Materials (Part I) - Elementary an Problems, 1940.

[37] Mallick PK. Fiber-reinforced composites: materials, manufacturing, and design. 3rd ed. Boca Raton, FL: CRC Press; 2008 (, [expanded and rev. ed.]).
[38] Gere JM. Mechanics of Materials. 6th edition. Thomson Learning, Inc, Stanford University; 2004.
[39] Rescalvo FJ, Duriot R, Pot G, Gallego A, Denaud L. Enhancement of bending properties of Douglas-fir and poplar laminate veneer lumber (LVL) beams with carbon and basalt fibers reinforcement. Constr Build Mater 2020;263:120185. https://doi.org/10.1016/j.conbuildmat.2020.120185.
[40] Vahedian A, Shrestha R, Crews K. Experimental and analytical investigation on CFRP strengthened glulam laminated timber beams: full-scale experiments. Compos Part B: Eng 2019;164:377–89. https://doi.org/10.1016/j.compositesb.2018.12.007.
[41] UNE-EN 1995-1-1, Eurocódigo5_Proyecto de estructuras de madera_parte 1-1, 2016.
[42] Ministerio de Fomento (Gobierno de España), Documento Básico SE: Seguridad Estructural, (n.d.). ⟨https://www.codigotecnico.org/pdf/Documentos/DBSE.pdf⟩.